



UNIVERSIDADE ESTADUAL DE CAMPINAS
SISTEMA DE BIBLIOTECAS DA UNICAMP
REPOSITÓRIO DA PRODUÇÃO CIENTÍFICA E INTELLECTUAL DA UNICAMP

Versão do arquivo anexado / Version of attached file:

Versão do Editor / Published Version

Mais informações no site da editora / Further information on publisher's website:

<https://www.tandfonline.com/doi/full/10.1080/00423114.2015.1125005>

DOI: 10.1080/00423114.2015.1125005

Direitos autorais / Publisher's copyright statement:

©2016 by Taylor & Francis. All rights reserved.

DIRETORIA DE TRATAMENTO DA INFORMAÇÃO

Cidade Universitária Zeferino Vaz Barão Geraldo

CEP 13083-970 – Campinas SP

Fone: (19) 3521-6493

<http://www.repositorio.unicamp.br>

Vehicle rollover avoidance by application of gain-scheduled LQR controllers using state observers

Vinicius F. Dal Poggetto  and Alberto L. Serpa 

DMC – Department of Computational Mechanics, FEM – School of Mechanical Engineering, UNICAMP – University of Campinas, Campinas, Brazil

ABSTRACT

Many researches have been conducted in the area of control applied to vehicle dynamics, aiming at reducing the possibility of the occurrence of the type of accident known as *rollover*. In this research, based on a common nonlinear model and its linearisation, a method for properly selecting matrices for solving the Riccati equation considering different speeds was proposed. The method showed in which ways speed really influences the choice of controller gains. By developing the dynamic equations for the yaw- and roll-coupled motions and modelling of controllers and state observers, it is possible to compare the efficacy of this control strategy using both linear and nonlinear simulations using Matlab. Significant results were obtained regarding the reduction of the rollover coefficient for a double-lane change manoeuvre at different speeds, thus indicating advantages of using this controller in practical cases.

ARTICLE HISTORY

Received 30 May 2014
Revised 14 September 2015
Accepted 21 November 2015

KEYWORDS

Rollover avoidance; active steering; LQR control; gain scheduling; yaw dynamics; vehicle safety

1. Introduction

In the later years, steering systems with electric assistance have been widely employed in the automotive industry. They consist of an auxiliary electric motor which is capable of correcting the steering angle which is fed into the steering system, leading to better performance, such as reducing undesired vibrations in the steering wheel. Another use of this type of system might be the compensation of steering angles to avoid accidents.

Dynamic models which describe the coupling between the yaw and roll motions of a vehicle have been used for demonstrating the advantages of active steering applied to vehicle safety. In [1–3], a linear model is used for describing this motion.

Aiming at the improvement of vehicle dynamics, proportional-integral-derivative controllers have been used [1–7] with output feedback. Techniques such as feedforward and invariance control have also been applied.[8,9] Optimal control has been previously investigated as well in [10]. Braking control strategies have also been studied, such as differential braking [11] and nonlinear braking.[2] Also, Ackermann and Odenthal [4] and Masár and Stöhr [12] have demonstrated the usefulness of gain-scheduled control, and linear-quadratic regulator (LQR) controllers have been previously employed for controlling roll–yaw dynamics as in [13].

Active components such as active anti-roll bars have been applied to improve the roll stability of single unit and articulated heavy vehicles.[14,15] Other control strategies, such as sliding mode control have also been developed,[16,17] where the authors have used active anti-roll bar and active suspension, respectively. Active anti-roll bars using a linear-quadratic controller have also been studied in [18]. Other active suspension strategies have also been applied, for example, in [19,20]. Specifically in [20], an approach using a dynamic rollover metric (Time-to-Rollover), which measures the time to an impending accident is also used.

Despite other strategies, active steering yields advantages regarding comfort and safety because of its continuous operating mode.[1] In this paper, an LQR controller with gain-scheduling and state-space observers is presented. Its parameters account for variations in the vehicle dynamics along a desired speed range. The performance of the controller is tested using linear and nonlinear simulations with a lane change manoeuvre.

In Section 2, a vehicle model is presented, as well as the representative scheme of the control system. Observers are modelled in Section 3, and controllers in Section 4. The application of the previous concepts are presented in Section 5, and its results in Section 6. Concluding remarks are presented in Section 7.

2. Vehicle model

2.1. Description

The presented model is described in several references.[2–4] Initially a nonlinear model is derived, from which a linear model is obtained. This model is used in this work to obtain speed-dependent state observers and controllers, which will later be assessed using both linear and nonlinear models. Figure 1 illustrates a frontal view of the vehicle model considered in this paper.

This model is similar to that presented in [21] and has been widely used in the field of control applied to vehicle dynamics. It comprises two rigid bodies: mass m_1 (unsprung

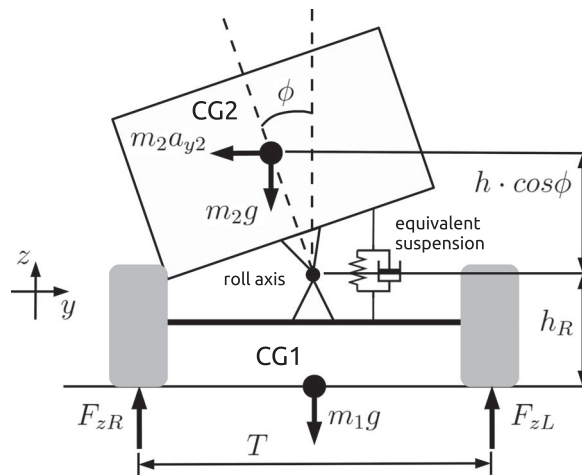


Figure 1. Front view of vehicle model.

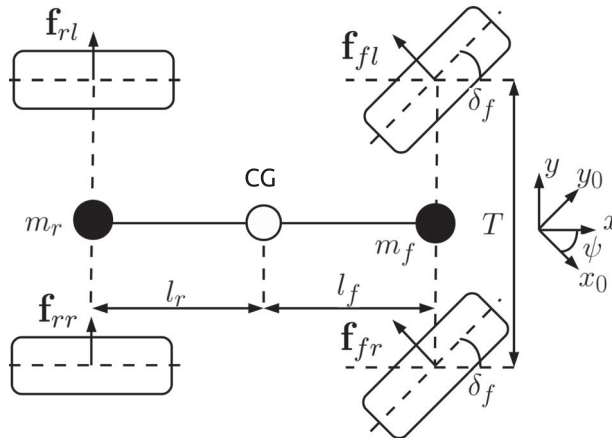


Figure 2. Upper view of vehicle model.

mass: composed of the vehicle frame, axles and wheels) and mass m_2 (sprung mass: vehicle body and parts that do not touch the ground). The model has the basic assumption of a fixed roll axis, which is parallel to the ground, in a height h_R . The sprung mass rolls about the roll axis, describing an angle ϕ with its vertical direction. The roll angle rate of change ($\dot{\phi}$) is one of the measured variables. The unsprung mass has a centre of gravity (CG1) which has little influence in the rolling movement, so it can be considered as lying on the ground. The centre of gravity of the sprung mass (CG2) has a fixed distance h to the roll axis, and total distance $h_R + h \cos \phi$ above the ground. The connection between the unsprung and sprung mass is made by the roll axis and an equivalent suspension, which is considered simply as a linear-relation spring–damper component (coefficients c_ϕ and d_ϕ) corresponding to rotational displacements.

Vertical reaction forces of vehicle wheels are depicted by F_{zR} and F_{zL} , with a distance of T , called track width. Each side vertical force can also be decomposed in frontal and rear wheel reactions, by taking into account the own weight vehicle distribution. Figure 2 shows an upper view of the vehicle. The total mass corresponding to the front axle is calculated as $m_f = m \cdot l_r / (l_f + l_r)$; the mass corresponding to the rear axle is $m_r = m \cdot l_f / (l_f + l_r)$, where l_f corresponds to the distance between the front axle and the centre of gravity of the vehicle, and l_r has the same property for the rear axle. The total mass of the vehicle is given by $m = m_1 + m_2$.

Important vehicle properties are also the yaw moment of inertia (J_z), roll moment of inertia of the sprung mass (J_{x2}) and the longitudinal speed of the vehicle (v_x).

2.2. Dynamic modelling

Newton–Euler equations can be applied to each separate body and can be used to analyse the yaw and roll motions. The four tyres are considered as force-generating elements. Figure 2 represents how lateral forces can be seen in the vehicle, and CG is the point in the xy plane where both CG1 and CG2 are located.

Tyre forces are nominated as f_{rl} (rear left tyre force), f_{rr} (rear right tyre force), f_{fl} (front left tyre force) and f_{fr} (front right tyre force). The angle between the global and local coordinate

system is the yaw angle (ψ). The rate of change of the yaw angle ($\dot{\psi}$) is another measured variable.

Each lateral force is a function of the slip angle of the corresponding tyre and its vertical reaction force, and this relation is based upon the level of detail needed. Tyre models can be considered nonlinear (in this case models described in [22] can be used) or linear (with a linear force to slip angle relation). Slip angles are defined as the difference between tyre's direction and its direction of travel. Slip angles are calculated as $\alpha_f = \delta_f - \beta_f$ for front wheels and $\alpha_r = -\beta_r$ for rear wheels (since $\delta_r \equiv 0$). Sideslip angles (β_f , β_r and β) are defined as the arctan between the longitudinal and lateral speeds at each point (front axle middle point, rear axle middle point and CG, respectively).

In this paper, a linear model was used to obtain the state-space model and for the controller design, but a nonlinear model was used for validating the controllers. In the case of linear tyre forces, these can be described as $F_y = c_f \alpha_f$ for front tyres and $F_y = c_r \alpha_r$ for rear tyres.[5] Henceforth, the variables c_f and c_r will be called front cornering stiffness and rear cornering stiffness. It is also common to include an additional parameter μ ($0 \leq \mu \leq 1$) in both front and rear tyres to take into account the road adhesion ($\mu = 0$ for a completely slippery surface, $\mu = 1$ for a dry road). In such a case, the lateral force can be expressed as $F_y = \mu c_f \alpha_f$ for front tyres and $F_y = \mu c_r \alpha_r$ for rear tyres.

If the same slip angles are considered for left and right sides (for front and rear), the model is called a *single-track model*, and each axle is collapsed into a point, turning the vehicle into a line. In this paper, the initial derivation was done for equal slip angles for the right and left side, but for the nonlinear case, separate slip angles were also calculated. Newton–Euler equations applied to this model leads to:

$$F_y = m\dot{v}_{y1} - hm_2 \frac{d^2}{dt^2}(\sin \phi) + mv_x \dot{\psi}, \quad (1)$$

$$M_z = J_z \ddot{\psi}, \quad (2)$$

$$J_{x2} \ddot{\phi} + c_\phi \dot{\phi} + d_\phi \dot{\phi} - m_2 \dot{v}_{y2} h \cos \phi - m_2 v_x \dot{\psi} h \cos \phi - m_2 v_{y2} \dot{\phi} h \sin \phi - m_2 g h \sin \phi = 0. \quad (3)$$

Vehicle parameters are described as

- h : distance between roll axis and CG of the sprung mass;
- h_R : height of roll axis;
- l_f : longitudinal distance between front axle and overall CG;
- l_r : longitudinal distance between rear axle and overall CG;
- m_1 : unsprung mass;
- m_2 : sprung mass;
- v_x : longitudinal speed of the vehicle;
- J_z : yaw moment of inertia;
- J_{x2} : sprung mass roll moment of inertia;
- c_ϕ : roll stiffness of equivalent suspension;
- d_ϕ : roll damping of equivalent suspension;
- μ : road adhesion coefficient;

and variables are

- F_y : total lateral force applied to the whole vehicle;
- M_z : total yaw moment applied to the whole vehicle;
- F_{zR} : vertical force at right side tyres;
- F_{zL} : vertical force at left side tyres;
- v_{y1} : unsprung mass lateral speed;
- v_{y2} : sprung mass lateral speed;
- ϕ : roll angle;
- ψ : yaw angle;
- δ_f : front wheels total steering angle.

Equations (1) and (2) refer to the effect of applying lateral forces or moments to the vehicle, while Equation (3) simply describes the rolling movement of the sprung mass when excited by lateral forces.

In order to transform all dynamic equations into state-space equations, one can linearise equations (1), (2) and (3) using small angles ($\phi \approx 0$), while considering tyre forces as being linear. Also, a state-space vector will be defined as

$$\mathbf{x} = \begin{Bmatrix} x_1 \\ x_2 \\ x_3 \\ x_4 \end{Bmatrix} = \begin{Bmatrix} \phi \\ v_{y1} \\ r \\ p \end{Bmatrix}, \quad (4)$$

where $r = \dot{\psi}$ and $p = \dot{\phi}$. Thus, these new variables yield the linear equations:

$$m\dot{x}_2 - hm_2\dot{x}_4 = -\frac{\mu(c_f + c_r)}{v_x}x_2 - \left[\frac{\mu(c_f l_f - c_r l_r)}{v_x} + mv_x \right] x_3 + \mu c_f \delta_f, \quad (5)$$

$$J_z \dot{x}_3 = -\frac{\mu(c_f l_f - c_r l_r)}{v_x}x_2 - \frac{\mu(c_f l_f^2 + c_r l_r^2)}{v_x}x_3 + \mu c_f l_f \delta_f \quad (6)$$

$$-hm_2\dot{x}_2 + (J_{x2} + h^2 m_2)\dot{x}_4 = -(c_\phi - m_2 gh)x_1 + hm_2 v_x x_3 - d_{\dot{\phi}} x_4, \quad (7)$$

In this paper, the selected output variables are $y_1 = \phi$, $y_2 = v_{y1}$, $y_3 = r$, $y_4 = p$ and $y_5 = \ddot{\phi}$. Another output variable is the rollover coefficient R , [3] which acts as an indicator of rollover tendency, defined as

$$R = \frac{F_{zR} - F_{zL}}{F_{zR} + F_{zL}}. \quad (8)$$

By analysing Equation (8), three cases may be noticed:

- if $R = 0$, then $F_{zR} = F_{zL}$: there is a balance between vertical forces in each side;
- if $R = -1$, then $F_{zR} = 0$: no force at the right side (vehicle rolls over);
- if $R = 1$, then $F_{zL} = 0$: no force at the left side (vehicle rolls over).

Quantities F_{zR} and F_{zL} can be expressed by taking equilibrium equations ($\sum F_z = 0$ and $\sum M_x = 0$) from Figure 1, solving for F_{zR} and F_{zL} . By doing this, one can substitute

F_{zR} and F_{zL} in Equation (8), and use the constants m_2 , m , T , h_R , h , v_x and g and state-space variables (ϕ, v_{y1} and r) to express R . This yields:

$$R = \frac{2m_2}{mT} \left\{ (h_R + h \cos \phi) \left[\frac{\dot{v}_{y1} + v_x r - h(d^2/dt^2)(\sin \phi)}{g} \right] + h \sin \phi \right\}. \quad (9)$$

Another variable of interest is the lateral acceleration of the sprung mass, represented by

$$a_{y2} = \dot{v}_{y1} + v_x r - h \frac{d^2}{dt^2}(\sin \phi). \quad (10)$$

It is important to notice that R and a_{y2} , as defined in Equations (9) and (10), are nonlinear equations. The small angle assumption will be applied to these equations later on to linearise them.

Finally, the outputs are $y_1 = \phi$, $y_2 = v_{y1}$, $y_3 = r$, $y_4 = p$, $y_5 = \ddot{\phi}$, $y_6 = R$ and $y_7 = a_{y2}$.

After comparing Equations (9) and (10), it is easy to note that the lateral acceleration of the sprung mass (a_{y2}) plays an important role in the rollover coefficient. Also, the total height of CG2 ($h + h_R$) affects the rollover tendency negatively. And finally, narrower track widths (small T) also make a vehicle more prone to rollover.

It is possible to linearise the nonlinear equations by using the small angle hypothesis, and in this case, the system can be written on a state-space form as

$$\dot{\mathbf{x}} = \mathbf{A}\mathbf{x} + \mathbf{B}\delta_f, \quad (11)$$

$$\mathbf{y} = \mathbf{C}\mathbf{x} + \mathbf{D}\delta_f, \quad (12)$$

with each matrix \mathbf{A} , \mathbf{B} , \mathbf{C} and \mathbf{D} written as

$$\mathbf{A} = \begin{bmatrix} 0 & 0 & 0 & 1 \\ a_{21} & a_{22} & a_{23} & a_{24} \\ 0 & a_{32} & a_{33} & 0 \\ a_{41} & a_{42} & a_{43} & a_{44} \end{bmatrix}, \quad (13)$$

where

- $a_{21} = \frac{-hm_2(c_\phi - ghm_2)}{-h^2m_2^2 + mh^2m_2 + J_{x2}m}$;
- $a_{22} = \frac{-\mu(c_f + c_r)(m_2h^2 + J_{x2})}{v_x(-h^2m_2^2 + mh^2m_2 + J_{x2}m)}$;
- $a_{23} = \frac{h^2m_2^2v_x}{-h^2m_2^2 + mh^2m_2 + J_{x2}m} - \frac{(mv_x + (\mu(c_f l_f - c_r l_r))/v_x)(m_2h^2 + J_{x2})}{-h^2m_2^2 + mh^2m_2 + J_{x2}m}$;
- $a_{24} = \frac{-d_\phi hm_2}{-h^2m_2^2 + mh^2m_2 + J_{x2}m}$;
- $a_{32} = \frac{-\mu(c_f l_f - c_r l_r)}{J_z v_x}$;
- $a_{33} = \frac{-\mu(c_f l_f^2 + c_r l_r^2)}{J_z v_x}$;
- $a_{41} = \frac{-m(c_\phi - ghm_2)}{-h^2m_2^2 + mh^2m_2 + J_{x2}m}$;
- $a_{42} = \frac{-hm_2\mu(c_f + c_r)}{v_x(-h^2m_2^2 + mh^2m_2 + J_{x2}m)}$;
- $a_{43} = \frac{hmm_2v_x}{-h^2m_2^2 + mh^2m_2 + J_{x2}m} - \frac{hm_2(mv_x + (\mu(c_f l_f - c_r l_r))/v_x)}{-h^2m_2^2 + mh^2m_2 + J_{x2}m}$;

$$\bullet a_{44} = \frac{-d_{\dot{\phi}} m}{-h^2 m_2^2 + mh^2 m_2 + J_{x2} m}.$$

$$\mathbf{B} = \begin{bmatrix} 0 \\ \frac{c_f \mu (m_2 h^2 + J_{x2})}{-h^2 m_2^2 + mh^2 m_2 + J_{x2} m} \\ \frac{c_f l_f \mu}{J_z} \\ \frac{c_f h m_2 \mu}{-h^2 m_2^2 + mh^2 m_2 + J_{x2} m} \end{bmatrix}, \quad (14)$$

$$\mathbf{C} = \begin{bmatrix} \mathbf{C}_{\phi} \\ \mathbf{C}_{vy1} \\ \mathbf{C}_r \\ \mathbf{C}_p \\ \mathbf{C}_{\ddot{\phi}} \\ \mathbf{C}_R \\ \mathbf{C}_{ay2} \end{bmatrix}, \quad (15)$$

$$\mathbf{D} = \begin{bmatrix} \mathbf{D}_{\phi} \\ \mathbf{D}_{vy1} \\ \mathbf{D}_r \\ \mathbf{D}_p \\ \mathbf{D}_{\ddot{\phi}} \\ \mathbf{D}_R \\ \mathbf{D}_{ay2} \end{bmatrix}. \quad (16)$$

It should be noted that \mathbf{C} – given by Equation (15) – is a 7×4 matrix. Thus, each of its lines consists of 1×4 matrices, representing the linear combination of states which relate to the desired output. The \mathbf{D} matrix is a 7×1 matrix.

Special attention should be given to R , which will be used for designing controller gains. After linearisation, one can write R as

$$R = \frac{2m_2}{mT} \left[(h_R + h) \frac{\dot{v}_{y1} + v_x r - h \ddot{\phi}}{g} + h \phi \right]. \quad (17)$$

Substituting state-space variables and its derivatives given by Equation (4), it is obtained

$$R = \frac{2m_2}{mT} \left[(h_R + h) \frac{\dot{x}_2 + v_x x_3 - h \dot{x}_4}{g} + h x_1 \right]. \quad (18)$$

Since state-space variables \dot{x}_2 and \dot{x}_4 were already expressed in terms of \mathbf{x} and δ_f using Equations (13) and (14), R might be expressed as

$$R = c_{R1} x_1 + c_{R2} x_2 + c_{R3} x_3 + c_{R4} x_4 + d_R \delta_f \quad (19)$$

where

- $c_{R1} = \frac{2hm_2(J_{x2}gm + c_\phi(h+h_R)(m-m_2) + gh_R(m_2^2 - mm_2))}{Tgm(-h^2m_2^2 + mh^2m_2 + J_{x2}m)}$;
- $c_{R2} = -\frac{2J_{x2}m_2\mu(c_f + c_r)(h+h_R)}{Tgmv_x(-h^2m_2^2 + mh^2m_2 + J_{x2}m)}$;
- $c_{R3} = -\frac{2J_{x2}m_2(h+h_R)\mu(c_{rf} - c_{rl})}{Tgmv_x(-h^2m_2^2 + mh^2m_2 + J_{x2}m)}$;
- $c_{R4} = \frac{2d_\phi hm_2(h+h_R)(m-m_2)}{Tgm(-h^2m_2^2 + mh^2m_2 + J_{x2}m)}$;
- $d_R = \frac{2J_{x2}\mu c_f m_2(h+h_R)}{Tgm(-h^2m_2^2 + mh^2m_2 + J_{x2}m)}$.

Finally, it is possible to express this relation in matrix form:

$$R = \mathbf{C}_R \mathbf{x} + \mathbf{D}_R \delta_f, \quad (20)$$

where

$$\mathbf{C}_R = [c_{R1} \quad c_{R2} \quad c_{R3} \quad c_{R4}], \quad (21)$$

$$\mathbf{D}_R = [d_R]. \quad (22)$$

At this point, it is important to notice that the dynamic behaviour of the vehicle is strongly dependent on the speed of the vehicle (v_x). Thus, there is not only one plant to be modelled, but rather a set of plants, with each plant determined for a specific speed. One could represent this dependance by writing $\mathbf{A} = \mathbf{A}(v_x)$, $\mathbf{B} = \mathbf{B}(v_x)$, $\mathbf{C} = \mathbf{C}(v_x)$ and $\mathbf{D} = \mathbf{D}(v_x)$ when writing state-space equations.

Despite the fact that seven variables have been selected as outputs, not all of them can be measured in a practical and cheap way. They are included in the mathematical modelling so they can be monitored throughout simulations. By using yaw-rate and roll-rate gyroscopic sensors, outputs y_3 and y_4 can be considered and measured in a practical way.

In order to represent this reduction in the number of outputs, a matrix \mathbf{S} can be introduced, being described by

$$\mathbf{S} = \begin{bmatrix} 0 & 0 & 1 & 0 & 0 & 0 & 0 \\ 0 & 0 & 0 & 1 & 0 & 0 & 0 \end{bmatrix}. \quad (23)$$

Thus, pre-multiplying \mathbf{C} and \mathbf{D} by \mathbf{S} is equivalent to selecting only its third and fourth lines. This product can be rewritten as the vector \mathbf{y}_{red} , a reduced output vector, described by

$$\mathbf{y}_{\text{red}} = \mathbf{C}_{\text{red}} \mathbf{x} + \mathbf{D}_{\text{red}} \delta_f, \quad (24)$$

where $\mathbf{C}_{\text{red}} = \mathbf{S}\mathbf{C}$ and $\mathbf{D}_{\text{red}} = \mathbf{S}\mathbf{D}$.

2.3. Block diagram

A block diagram is depicted in Figure 3, representing signal routing and subsystem assembly.

It is possible to observe that signal δ_L , the steering wheel angle, is the input of the system. This angle becomes δ_s , the effective steering angle, after the steering column (represented

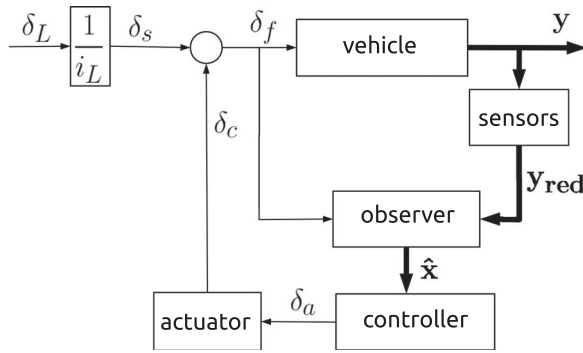


Figure 3. States observation and feedback scheme.

by the steering ratio i_L). The angle δ_s is then summed with the additional steering angle δ_c , to become the front wheels steering angle δ_f .

Every possible output y can be determined by the system dynamics (vehicle block in Figure 3). Gyroscopic sensors are able to retrieve outputs contained in vector y_{red} , which can then be fed into the observer, along with the instantaneous value of δ_f . The vehicle states can then be properly estimated and used with the LQR controller for determining the controlled steering angle δ_a . This controlled angle can then be considered into the actuator dynamics (modelled as a low-pass filter with a 5 Hz cut-off frequency, as described in [4]) and turned into the additional steering angle δ_c .

Since only two states (yaw-rate and roll-rate) are measured, the problem becomes to obtain all states from the model in order to feedback a suitable control signal. This can be achieved by using state-space observers able to estimate all states from the only two direct measures provided by y_{red} .

3. Design of state observers

By incorporating matrix \mathbf{S} into the vehicle modelling, one should also include it in the observer equations. Thus, the observer dynamic equation which describes state estimation is given by [23]

$$\dot{\hat{\mathbf{x}}} = \mathbf{A}\hat{\mathbf{x}} + \mathbf{B}\delta_f + \mathbf{L}(y_{\text{red}} - \mathbf{C}_{\text{red}}\hat{\mathbf{x}}), \quad (25)$$

where $\hat{\mathbf{x}}$ is the estimate for \mathbf{x} .

Since the plant is dependent on its operating speed, a set of state observers should also be developed for determining the model states in several different speeds. In practical cases, the vehicle speed is a continuous variable, so gains should be available for virtually every speed. It is not possible to calculate observer gains for an infinite number of vehicle speeds, so these gains are calculated for a finite set of speeds and then interpolated, leading to curves of gains as functions of speed. It is also very important to determine whether the system has a complete observability.

Observer gain matrix \mathbf{L} is calculated here with poles being placed at locations equal to four times matrix \mathbf{A} eigenvalues. After calculating observer gains for a finite set of speeds, state-space observer gains are interpolated for a virtually continuous set of speeds, making it possible to retrieve observer gains for any desired speed.

Once all observer gains can be retrieved for each speed, all states can be estimated and it is possible to apply a control law which will provide an additional steering angle to the steering column.

4. Design of controllers

The controller gains should also be determined while considering the speed dependence of the vehicle dynamics, creating controller gain curves in a speed-dependent manner. In this paper, LQR controllers were used, [24] using estimated states from the observers. These controllers will take the form:

$$\mathbf{u}(t) = -\mathbf{K}\hat{\mathbf{x}}(t). \quad (26)$$

An adaptive controller can be defined as a controller with adjustable parameters and a technique for adjusting its parameters. According to [25], it is possible to consider four types of adaptive systems: gain-scheduling, model-reference adaptive control, self-tuning regulators and dual control. By this point of view, the first adaptive concept, gain-scheduling, was used in this work. In this way, \mathbf{K} in Equation (26) could actually be described by $\mathbf{K} = \mathbf{K}(v_x)$. For every desired speed, an LQR equation should be applied, determining all controller gains (k_ϕ , $k_{v_{y1}}$, k_r and k_p). In order to determine \mathbf{K} , Riccati equation should be solved taking into account the minimisation of J given by

$$J = \int_0^\infty (\mathbf{x}^T \mathbf{Q} \mathbf{x} + \mathbf{u}^T \mathbf{R} \mathbf{u}) dt, \quad (27)$$

where matrices \mathbf{Q} and \mathbf{R} are weighting matrices for states (\mathbf{x}) and control signal ($\mathbf{u} = \delta_f$), respectively. By using terms from Equations (21) and (22), matrices \mathbf{Q} and \mathbf{R} can be chosen as

$$\mathbf{Q} = \begin{bmatrix} q_{11} & 0 & 0 & 0 \\ 0 & q_{22} & 0 & 0 \\ 0 & 0 & q_{33} & 0 \\ 0 & 0 & 0 & q_{44} \end{bmatrix}, \quad (28)$$

$$\mathbf{R} = \rho [d_R^2], \quad (29)$$

where $q_{11} = c_{R1}^2$, $q_{22} = c_{R2}^2$, $q_{33} = c_{R3}^2$ and $q_{44} = c_{R4}^2$. These terms, present in Equations (28) and (29), are described right after Equation (19).

Parameter ρ in Equation (29) represents a weighting factor for the control signal, which is determined by experimenting on several values, adjusting it until there is a compromise between good safety and low controller intrusiveness. Lower values of ρ indicate a low *cost* for control effort, so the controller could actuate intensively. On the other hand, higher values for ρ indicate the controller should act less, thus emphasising smoothness. Examining Equation (19), it is possible to see that the terms c_{R2} and c_{R3} are functions of the inverse of the vehicle's speed. Thus, both terms q_{22} and q_{33} would tend to infinity as v_x approaches zero, and would converge to zero for large values of v_x . Other terms are not speed-dependent. It seems reasonable to consider both matrices \mathbf{Q} and \mathbf{R} as constant, with its elements equal to those obtained using asymptotic values of v_x , thus avoiding singularities at speeds close to zero.

The same procedure of calculation of controller gains for a finite number of values of v_x and the interpolation of these gains for a set of speeds is used here (as for state observers). Once state observers and controllers have been properly defined for a continuous set of the speeds of the vehicle, it is possible to study the system from a closed-loop perspective.

5. Closed-loop system analysis

After combining all subsystems as in Figure 3, it is important to check for stability in the possible speeds for the sake of safety. This can be done by creating a closed-loop form of the system, and taking the largest real part of the systems' eigenvalues. After verifying system stability, different conditions can be simulated using both linear and nonlinear simulations.

6. Results

Now considering a vehicle with the parameters (as in [4]) $c_f = 582$ kN/rad, $c_r = 783$ kN/rad, $h = 1.15$ m, $h_R = 0.68$ m, $l_f = 1.95$ m, $l_r = 1.54$ m, $T = 1.86$ m, $m_1 = 1813$ kg, $m_2 = 12487$ kg, $J_z = 34917$ kg · m², $J_{x2} = 24201$ kg · m², $c_\phi = 457$ kN · m/rad and $d_{\dot{\phi}} = 100$ kN · m/rad/s, some simulations can be performed (using $\mu = 1$ and $g = 9.81$ m/s²).

Open-loop stability is related to the understeer coefficient [26]:

$$K_v = \frac{W_f}{c_f} - \frac{W_r}{c_r}, \quad (30)$$

where $W_f = m_f g$ and $W_r = m_r g$. Since $K_v > 0$ for this vehicle, the system does not present open-loop instability. This can also be confirmed for some speed values in Figure 4, where real and imaginary parts of the poles are plotted for several speeds (from 1 to 101 km/h, with a 10 km/h step). It is important to mention that stability should not be confused with the avoidance of rollover, which corresponds only to normal load redistribution.

Steering angles can be applied into the steering wheel (using both linear and nonlinear simulations) to evaluate the rollover tendency of the vehicle. The intended manoeuvres may be defined as two complete cycles of a sinusoidal function, having opposite phases, with each frequency being defined by an equivalent 3.5 m lateral displacement of the linear case. An example of an input manoeuvre is presented in Figure 5.

The differences between linear and nonlinear simulations consist basically of a small angle approximation, which results in linearisation of dynamic equations and tyre forces (small slip angles). Linear models can be simulated with Matlab, while nonlinear simulations were performed using Simulink module because of its easy use regarding nonlinear simulations and connections. Nonlinear simulations include Pacejka tyre models [22] for representing force/slip angles relations and nonlinear differential equations solving. Also, cornering stiffness is not constant and the normal load redistribution, influencing the generation of lateral forces, is considered. Also, it is important to notice that only the linear model is used to determine observer and controller gains, but the resulting observers and controllers are applied to the nonlinear model for assessing its efficacy.

In this paper, the design of state-space observers has been done using speeds between 1 and 101 km/h (considered a broad range of possible speeds for this vehicle) with a 10 km/h

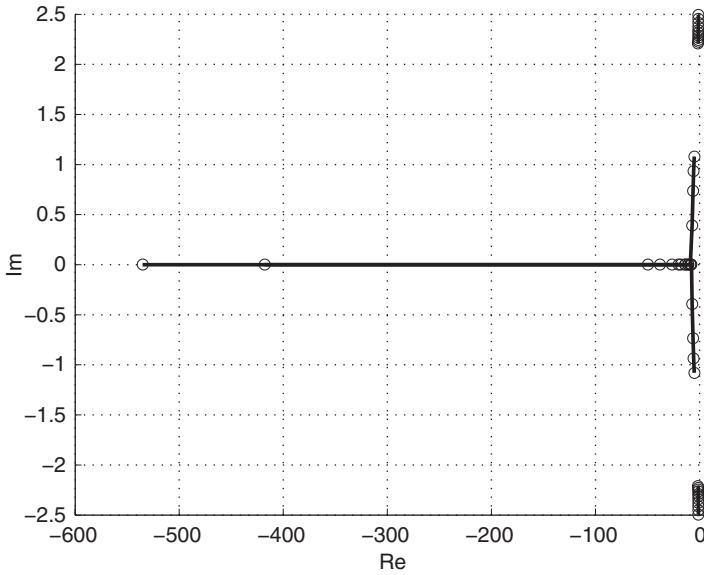


Figure 4. Open-loop real and imaginary parts of the poles as a function of speed.

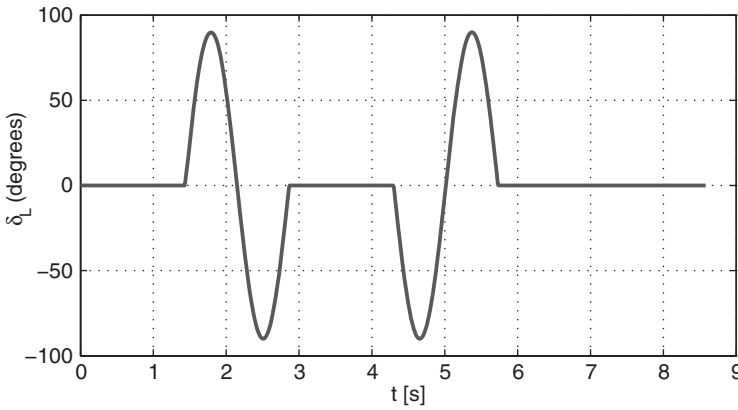


Figure 5. Manoeuvre input # 2.

step. This has been achieved using this set of calculated gains with a 0.01 m/s resolution. An example of the dependance between observer gains and the speed of the vehicle is depicted in Figure 6. Observability has been assessed for the design speeds, proving the system to be completely observable at them.

Controller gains were obtained with a value of $\rho = 2.5$ found by comparing the controller performance in various situations. As discussed previously in Section 4, $q_{22} = c_{R2}^2$ and $q_{33} = c_{R3}^2$ can be considered initially as speed-dependent quantities (c_{R2} and c_{R3} are speed-dependent), but this would lead to singularities when v_x reaches zero. To avoid this, matrices \mathbf{Q} and \mathbf{R} were considered constant.

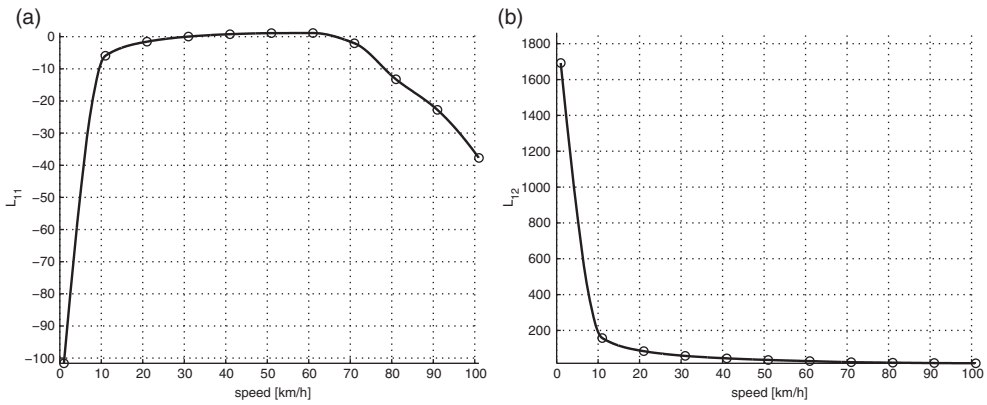


Figure 6. Two observer gains as functions of speed.

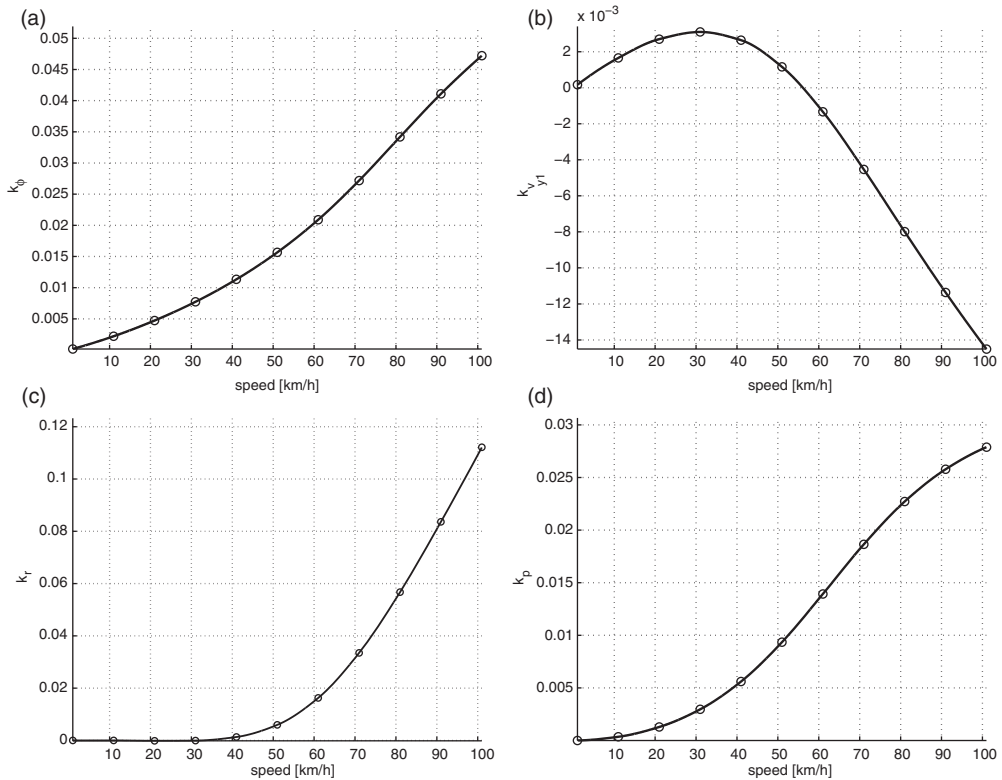


Figure 7. Controller gains as functions of speed.

By solving the Riccati equation for several speeds (the same used for the state observers design), it is possible to determine the controller gains at these selected speeds. Once again, by interpolating these points, curves shown in Figure 7 were obtained.

Closed-loop system stability was verified using a step of 0.01 m/s for the v_x speed. This allowed to verify that every possible closed-loop system is stable, since there was not an

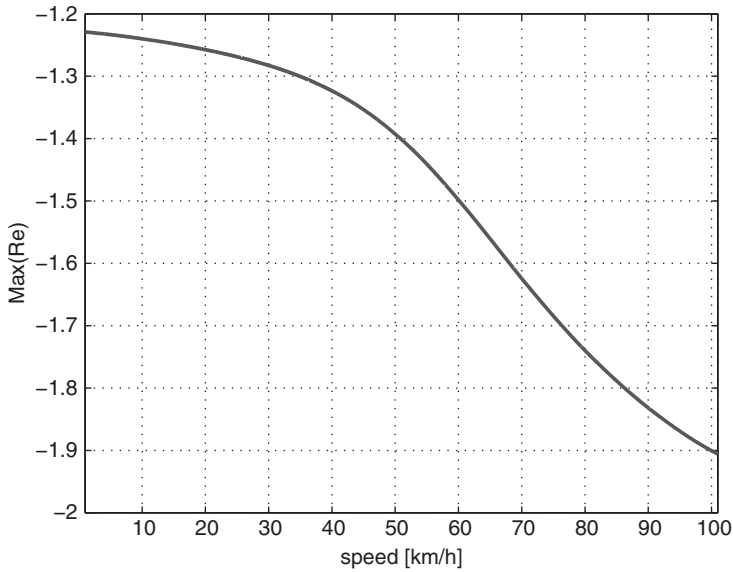


Figure 8. Maximum real part of closed-loop poles versus speed variation with a step of 0.01 m/s.

Table 1. Input conditions.

Manoeuvre #	Speed (km/h)	Frequency (Hz)
1	40	0.4060
2	70	0.6980
3	100	0.9578

eigenvalue with a positive real part for every point in the whole speed span with this fine discretisation in the speed. This result can be checked in Figure 8.

Since closed-loop stability was verified for the interest speed range, manoeuvres can now be evaluated. In this paper, three manoeuvres were tested using 40, 70 and 100 km/h speeds. The steering wheel amplitude was kept at 90° and the steering ratio $i_L = 15$. These conditions are summarised in Table 1.

Results are summarised in Table 2, for both linear and nonlinear cases of simulation. In Table 2, the term $\Delta|R|_{\max}$ has been calculated as the difference between the maximum values of $|R|$ in the controlled and uncontrolled cases. In situations where rollover occurred, $|R|_{\max}$ has been calculated considering the time instant before the rollover happened ($|R| = 1$) in each case. As it may be seen, for speeds of 40 and 70 km/h, the condition $R = 1$ occurred, indicating the possibility of rollover.

Simulations have also been performed considering some parameters' uncertainties:

- sprung mass uncertainty ($\Delta m_2 = \pm 0.10 m_2$): accounting for variations in the sprung mass, and its effect in yaw moment of inertia, sprung mass roll moment of inertia (under the hypothesis of a constant radius of gyration, which assumes uniform distribution of the mass variation) and cornering stiffness (for both front and rear tyres, each tyre normal force has to be again calculated);

Table 2. Rollover prediction for nominal values.

Type	Manoeuvre #	Prevented rollover?	$\Delta R _{\max}$
Linear model	1	No need	-0.02
	2	No	NA
	3	Yes	-0.08
Nonlinear model	1	No need	-0.02
	2	Yes	-0.03
	3	Yes	-0.12

Table 3. Sprung mass uncertainty effect on nonlinear simulations.

Manoeuvre #	$(\Delta m_2 = -0.10m_2)$		(Nominal)		$(\Delta m_2 = +0.10m_2)$	
	Prevented rollover?	$\Delta R _{\max}$	Prevented rollover?	$\Delta R _{\max}$	Prevented rollover?	$\Delta R _{\max}$
1	No need	-0.02	No need	-0.02	No need	-0.02
2	Yes	-0.04	Yes	-0.03	Yes	-0.02
3	Yes	-0.14	Yes	-0.12	Yes	-0.12

Table 4. Cornering stiffness effect on nonlinear simulations.

Manoeuvre #	$(\Delta c_f = -0.10c_f, \Delta c_r = -0.10c_r)$		(Nominal)		$(\Delta c_f = +0.10c_f, \Delta c_r = +0.10c_r)$	
	Prevented rollover?	$\Delta R _{\max}$	Prevented rollover?	$\Delta R _{\max}$	Prevented rollover?	$\Delta R _{\max}$
1	No need	-0.01	No need	-0.02	No need	-0.02
2	Yes	-0.09	Yes	-0.03	No	0.01
3	Yes	-0.21	Yes	-0.12	Yes	-0.05

- cornering stiffness ($\Delta c_f = \pm 0.10c_f$ and $\Delta c_r = \pm 0.10c_r$): considering this variation isolated, with no variation of other parameters.

It is important to notice that only nominal values were used for observer and controller designs. The sprung mass uncertainty has been shown (Table 3) not to be detrimental to controller performance, since only a slight variation in results could be noticed. On the other hand, this method was not successful for a robust performance due to changes only in the cornering stiffness values (Table 4).

A set of results from the nonlinear simulations (70 km/h speed) is presented in Figure 9, where the uncontrolled case is indicated through dashed lines, and the controlled case with continuous ones.

Figure 9(a) shows the relation between front wheels' steering angle (δ_f), the steering angle after the steering column (δ_s) and the additional steering angle yielded by the controller and actuator set (δ_c). The controller tries to make the front wheels' steering angle to be applied in a smoother way, and do this by trying to counter rough actions coming from the driver. As previously stated, the controller has to be adjusted (through the parameter ρ), in order to maintain an acceptable intrusiveness regarding driver's acceptance. Also, because of the way the controller is designed, its actuation is more meaningful in situations which the vehicle is prone to rollover (as seen from Equations (27) and (20)).

Figure 9(b) shows the controlled vehicle (continuous line) versus the uncontrolled vehicle (dashed line). Both vehicles start out describing the curve in the same way, but the uncontrolled vehicle reaches $R = 1$ very soon, and the simulation stops. The controlled

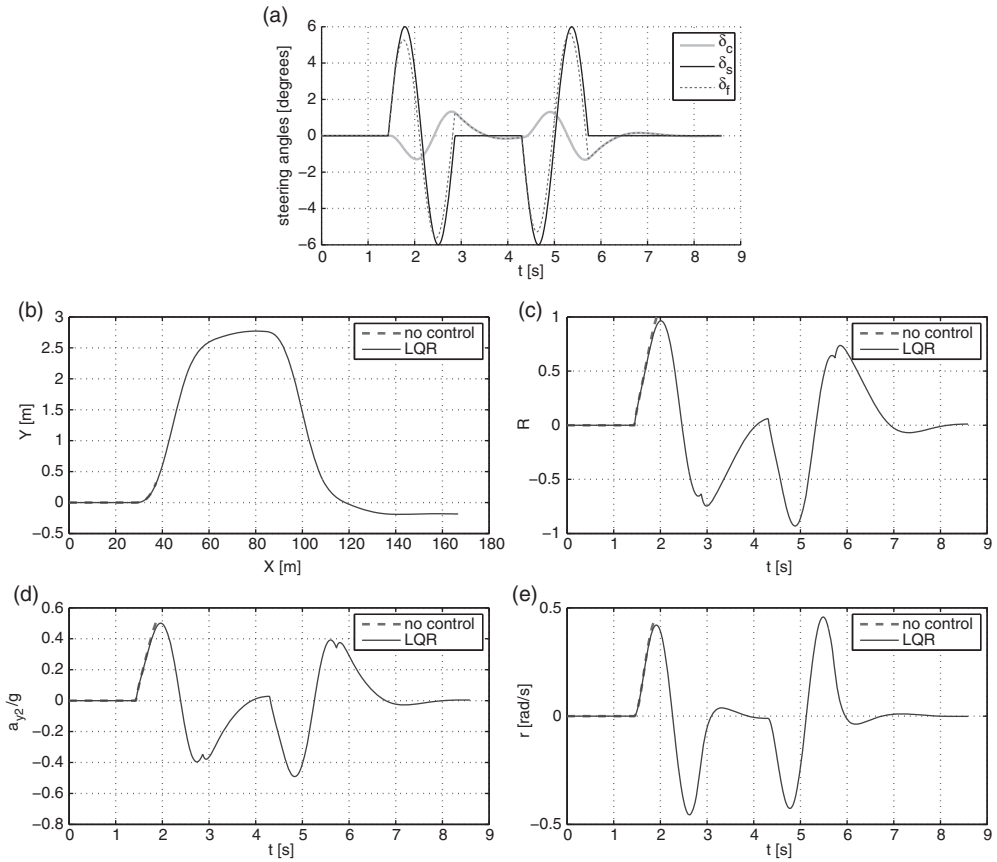


Figure 9. Nonlinear simulation results.

vehicle does not roll over and finishes its manoeuvre. It is possible to see in Figure 9(c) the time instant where the rollover occurs for the uncontrolled vehicle (near $t = 2$ s). The controlled vehicle has a high value of the rollover coefficient, but does not reach $R = 1$.

It is important to notice (Figures 9(d) and 9 (e)) that the lateral sprung mass acceleration and yaw rate are kept at low levels when the controller acts. Also, since no significant difference between the controlled and uncontrolled cases between $t = 0$ s and $t = 2$ s is verified, this can be considered an evidence that the control system does not interfere significantly until it is required to act.

The sprung mass roll angles can be observed in Figure 10 for the three manoeuvre speeds. In these nonlinear simulations, the roll angles remain small according to the initial small angle hypothesis.

From a dynamical point of view, adding an additional controlled steering angle to the system slightly changes vehicle response taking into account how prone a vehicle is to rollover in that moment, that is, if the vehicle is operating at a low speed or with little lateral acceleration, the control system does not change the steering angle in a significant manner.

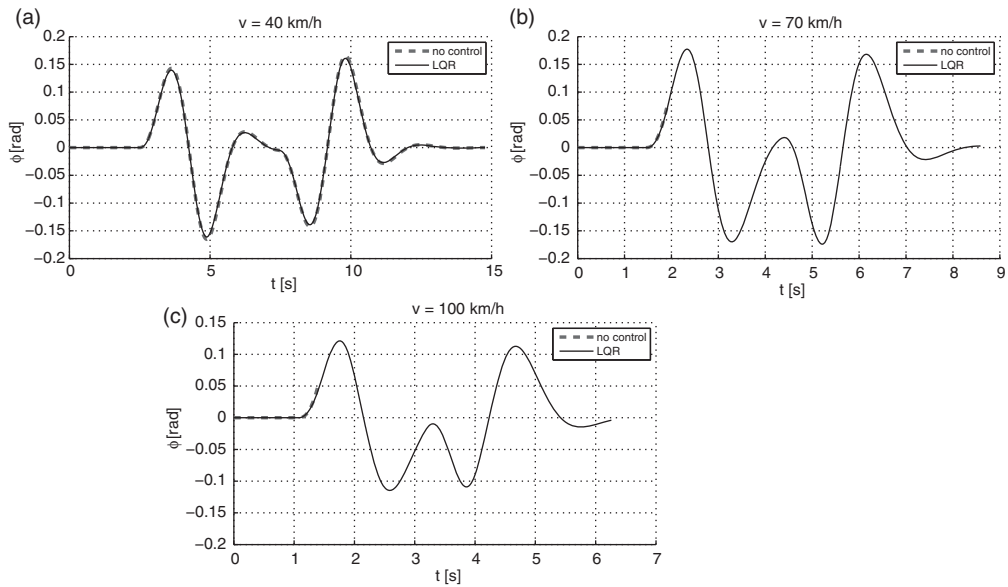


Figure 10. Roll angles results for nonlinear simulations.

7. Conclusions

Active steering with variable state observer and controller gains was investigated in this work, and a method for properly selecting matrices for solving the Riccati equation under different speeds was proposed. It was possible to show that state observers work well under the investigated circumstances.

Stability has been discussed by showing that the real parts of poles lay in a stable region for a fine speed numerical discretisation step. This numerical investigation was considered suitable for practical simulation purposes in this work, particularly when considering the nonlinear model simulations. A proper proof of stability may be investigated in the future trying to consider the speed variation formally in the mathematical problem formulation.

Also, although matrices \mathbf{Q} and \mathbf{R} as defined in the Riccati equation are speed-dependent due to two terms (q_{22} and q_{33}), these terms were shown to rapidly converge to zero, leaving the speed dependence only to state-space matrices \mathbf{A} and \mathbf{B} . The interpolation of both observer and controller gains over the speed range seems to work fairly well, showing this method yields smooth curves. Also, the controller has proved itself stable, not leading to unexpected behaviours on the analysed situations. The resulting closed-loop system had its performance tested with linear and nonlinear simulations, showing good performance and avoiding rollover accidents.

A gain-scheduling strategy for the design of both state observer and controller was verified in this work. It has been shown that by using only simple vehicle data (such as mass, inertia moments, etc.) as inputs for calculating gains on certain speeds, it is possible to interpolate these gains for several other speeds, leading to an active steering system suited for the prevention of rollover accidents. The sprung mass uncertainty, $\pm 10\%$, has been shown not to be detrimental to controller performance; however, robust performance was sensitive to cornering stiffness uncertainty values (also $\pm 10\%$).

Disclosure statement

No potential conflict of interest was reported by the authors.

ORCID

Vinicius F. Dal Poggetto  <http://orcid.org/0000-0003-0862-6270>

Alberto L. Serpa  <http://orcid.org/0000-0001-7380-3099>

References

- [1] Ackermann J, Bünte T, Odenthal D. Advantages of active steering for vehicle dynamics control. In: Proceedings of 32nd International Symposium on Automotive Technology and Automation; Croydon, England; 1999. p. 263–270.
- [2] Odenthal D, Bünte T, Ackermann J. Nonlinear steering and braking control for vehicle rollover avoidance. In: Proceedings of European Control Conference; Karlsruhe, Germany; 1999. p. 598–603.
- [3] Ackermann J, Odenthal D. Robust steering control for active rollover avoidance of vehicles with elevated centre of gravity. In: Proceedings of International Conference on Advances in Vehicle Control and Safety; Amiens, France; 1998.
- [4] Ackermann J, Odenthal D. Damping of vehicle roll dynamics by gain scheduled active steering. In: Proceedings of European Control Conference; Karlsruhe, Germany; 1999. p. 1041–1042.
- [5] Ackermann J, Forschungsanstalt D. Yaw disturbance attenuation by robust decoupling of car steering. *Control Eng Pract.* 1997;5:1131–1136.
- [6] Ackermann J, Walter W, Bünte T. Automatic car steering using robust unilateral decoupling. In: Proceedings of International Conference on Advances in Vehicle Control and Safety; Salerno, Italy; 2004.
- [7] Solmaz S, Corless M, Shorten R. A methodology for the design of robust rollover prevention controllers for automotive vehicles: part 2 – active steering. In: American Control Conference; New York City, USA; 2007. p. 1606–1611.
- [8] Ackermann J, Bünte T. Handling improvement for robustly decoupled car steering dynamics. In: Proceedings of 4th IEEE Mediterranean Symposium on New Directions in Control & Automation; Chania, Greece; 1996. p. 83–88.
- [9] Wollherr D, Mareczek J, Buss M, Schmidt G. Rollover avoidance for steerable vehicles by invariance control. In: Proceedings of the 2001 European Control Conference; Porto, Portugal; 2001. p. 3522–3527.
- [10] Lin RC, Cebon D, Cole DJ. Optimal roll control of a single-unit lorry. *Inst Mech Eng D: J Automob Eng.* 1996;210:45–56.
- [11] B-C Chen, Peng H. Differential-braking-based rollover prevention for sport utility vehicles with human-in-the-loop evaluations. *Veh Syst Dyn.* 2001;36:359–389.
- [12] Masár I, Stöhr E. Gain-scheduled LQR-control for an autonomous airship. In: Proceedings of the 18th International Conference on Process Control; Tatranská Lomnica, Slovakia; 2011. p. 197–204.
- [13] Shariatmadar S, Manteghi M, Tajdari M. Enhancement of articulated heavy vehicle stability by optimal linear quadratic regulator (LQR) controller of roll-yaw dynamics. *Int J Automot Eng ISAE.* 2012;2:124–131.
- [14] Sampson DJM. Active roll control of articulated heavy vehicles [PhD thesis]. Cambridge University Engineering Department; 2000.
- [15] Lin RC, Cebon D, Cole DJ. Active roll control of articulated vehicles. *Veh Syst Dyn.* 1996;26:17–43.
- [16] Chu D, Ma J, Li G. Active roll stability control for vehicle rollover prevention with combined dynamics modeling. *Int J Adv Comput Technol.* 2012;4:26–35.

- [17] Chu D, Lu X, Wu C, Hu Z, Zhong M. Smooth sliding mode control for vehicle rollover prevention using active antiroll suspension. *Math Problems Eng.* 2015; 8. Article ID 478071.
- [18] Varga B, Németh B, Gáspár P. Design of anti-roll bar systems based on hierarchical control. *J Mech Eng.* 2015;61:374–382.
- [19] Westhuizen SF, Els PS. Slow active suspension control for rollover prevention. *J Terramechanics.* 2013;50:29–36.
- [20] Yu H, Güvenc L, Özgüner U. Heavy-duty vehicle rollover detection and active roll control. *Veh Syst Dyn.* 2008;46:451–470.
- [21] Segel L. Theoretical prediction and experimental substantiation of the response of the automobile to steering control. *Proc Inst Mech Eng: Automob Div.* 1956;10:310–330.
- [22] Pacejka HB. *Tyre and vehicle dynamics.* Burlington: Elsevier; 2005.
- [23] Ogata K. *Modern control engineering.* New Jersey: Prentice-Hall Englewood Cliffs; 1970.
- [24] Shahian B, Hassul M. *Control system design using Matlab.* New Jersey: Prentice-Hall; 1993.
- [25] Aström K, Wittenmark B. *Adaptive control.* Mineola: Courier Corporation; 2013.
- [26] Gillespie TD. *Fundamentals of vehicle dynamics.* Warrendale: Society of Automotive Engineers; 1992.